

Submitted to Ap.J.

Detection of Cosmic Microwave Background Anisotropy by the Third Flight of MSAM

E. S. Cheng¹, D. A. Cottingham², D. J. Fixsen³, A. B. Goldin⁴, C. A. Inman^{4,1}, L. Knox⁵, M. S. Kowitt^{1,4}, S. S. Meyer⁴, J. L. Puchalla¹, J. E. Ruhl^{4,6}, and R. F. Silverberg¹

ABSTRACT

The third flight of the Medium Scale Anisotropy Measurement (MSAM1), in June 1995, observed a new strip of sky, doubling the sky coverage of the original MSAM1 dataset. MSAM1 observes with a 0.5° beam size in four bands from $5\text{--}20\text{ cm}^{-1}$. From these four bands we derive measurements of cosmic microwave background radiation (CMBR) anisotropy and interstellar dust emission. Our measurement of dust emission correlates well with the $100\text{ }\mu\text{m}$ *IRAS* Sky Survey Atlas; from this comparison we determine an effective emissivity spectral index between $100\text{ }\mu\text{m}$ and $444\text{ }\mu\text{m}$ of 1.46 ± 0.28 . Analysis of our measurement of CMBR anisotropy shows that for Gaussian-shaped correlation functions with $\theta_c = 0.3^\circ$, we place a limit on total rms anisotropy of $2.2 \times 10^{-5} < \Delta T/T < 3.9 \times 10^{-5}$ (90% confidence interval, including calibration error). The band-power limits are $\langle \delta T \rangle \equiv \langle l(l+1)C_l/2\pi \rangle^{1/2} = 50_{-11}^{+16}\text{ }\mu\text{K}$ at $l = 160$, and $\langle \delta T \rangle = 65_{-13}^{+18}\text{ }\mu\text{K}$ at $l = 270$ (1σ limits, including calibration error). The corresponding limits with statistical errors only are $\langle \delta T \rangle = 50_{-9}^{+13}\text{ }\mu\text{K}$ and $\langle \delta T \rangle = 65_{-10}^{+14}\text{ }\mu\text{K}$ respectively. These measurements are consistent with a standard adiabatic cold dark matter model; we discuss constraints on h , n , and the redshift of reionization.

¹NASA/Goddard Space Flight Center, Laboratory for Astronomy and Solar Physics, Code 685.0, Greenbelt, MD 20771

²Global Science and Technology, Inc., NASA/GSFC Laboratory for Astronomy and Solar Physics, Code 685.0, Greenbelt, MD 20771

³Applied Research Corporation, NASA/GSFC Laboratory for Astronomy and Solar Physics, Code 685.0, Greenbelt, MD 20771

⁴University of Chicago, 5640 S. Ellis St., Chicago, IL 60637

⁵CITA, University of Toronto, Toronto, Ontario M5S 3H8, Canada

⁶Department of Physics, University of California, Santa Barbara, CA 93106

Subject headings: balloons — cosmic microwave background — cosmology: observations — infrared: ISM: continuum

1. Introduction

The Medium Scale Anisotropy Measurement (MSAM) is an experiment to measure anisotropy in the cosmic microwave background radiation (CMBR) at an angular scale near $0^{\circ}5$. The first two flights of MSAM1, reported in Cheng *et al.* 1994 (Paper I) and Cheng *et al.* 1996 (Paper II), both observed the same field to demonstrate the repeatability of our measurements. The detailed comparison, showing consistency between these two measurements, was reported in Inman *et al.* 1997. To increase sky coverage and consequently increase sensitivity to the CMBR anisotropy power spectrum, the third flight of MSAM1 (MSAM1-95) measured a new field using the same observing method. This paper reports initial results from this third flight. We will report results from the combined dataset of all three flights in a future paper.

Some recent measurements of CMBR anisotropy have begun to hint at the shape of the correlation function near $0^{\circ}5$. Netterfield *et al.* 1997, from analysis of new measurements from their Saskatoon experiment (SK95), report a rise from $l \approx 90$ to 240; Platt *et al.* 1997 report that new measurements with Python III are consistent with a flat power spectrum from $l \approx 90$ to 180. Analysis of such measurements in conjunction with the DMR maps have begun to suggest what area of cosmological parameter space is viable. Bond and Jaffe 1997 have analyzed the Saskatoon data along with SP94 and DMR, and find that with a number of parameters fixed they can put interesting limits on others, e.g. H_0 . In this letter we report similar initial results based on the MSAM1-95 data.

2. Instrument and Observations

A detailed description of the MSAM1 instrument can be found in Fixsen *et al.* 1996b. We give a brief overview here. MSAM is a balloon-borne 1.4 m off-axis Cassegrain telescope which forms a beam of width $\sim 0^{\circ}5$. A three-position chopping secondary throws the beam $\pm 0^{\circ}7$; we run this chopper at 2 Hz. The MSAM1 detector system has four spectral channels at 5.7, 9.3, 16.5, and 22.5 cm^{-1} , each with a width of $\sim 1\text{--}2 \text{ cm}^{-1}$. The detectors are sampled at 32 Hz: 4 times for each of 4 positions of the secondary mirror, for a total of 16

samples per chopper cycle. Pointing is determined with a star camera and gyroscope. The configuration of the gondola for the 1995 flight is unchanged from the 1994 flight.

The third flight of MSAM1 was launched from the National Scientific Balloon Facility in Palestine, Texas at 23:54 UT 01 Jun 1995. CMBR field observations were taken at altitudes of 37.5 – 40 km. During the flight, we observed Mars, Jupiter, and Saturn to calibrate the instrument (these observations are reported in detail in Goldin *et al.* 1996). To measure anisotropy in the CMBR, we observed a strip of sky at $\delta \sim 80^\circ.5$ from $\alpha \sim 14^\text{h}2$ to $19^\text{h}5$ over the period 04:20 to 09:22 UT. We terminated the observation at that time because we were entering a region of increased emission from Galactic dust. This field parallels the MSAM1-92/MSAM1-94 field at a distance of $1^\circ.5$ in declination.

The observing method for our CMBR scans is the same as that described in papers I and II, adjusted for the faster sky motion at the lower declination. We begin with the telescope pointed at a spot at $\delta = 80^\circ.5$, $25'$ east of the meridian. We scan in azimuth a distance of $\pm 47'$ on the sky with a period of 60 s and track sky rotation until the center of the scan is $25'$ west of the meridian. This takes about 20 min. We then pause briefly for a star camera picture, move $50'$ to the right (so we are again $25'$ east of the meridian), and start a new scan. During the flight we completed 15 scans (integration time on the first scan was only 14 min).

3. Data Analysis

The reduction of the data consists of the following steps. The detector data are contaminated by spikes caused by cosmic rays striking the detectors; we remove these spikes. The data are calibrated by our observation of planets, and are analyzed to provide measurements of brightness in our four spectral channels as a function of sky position. These are then fit to a spectral model to produce measurements of CMBR anisotropy and dust optical depth. These analyses and their results are described in the following sections.

3.1. Detector Data Reduction

The observed signal is noise plus a convolution of the radiation incident on the bolometer with the transfer function of the bolometers, electronics and sampling. To reconstruct the incident signal optimally (with minimum variance) from that observed we apply a Wiener filter to the data. The detector data contain spikes, generally consistent with cosmic rays striking the bolometers. In the unfiltered time stream, a cosmic ray hit

contaminates ~ 30 time samples. The Wiener filter compresses this mostly into one sample with some ringing present in the adjacent samples — all of which are cut. The extent of the ringing and therefore the breadth of the cut depends on the glitch amplitude; a typical breadth of the cut is 10 samples. In addition, an interval of 12 s around each telemetry dropout is removed. A total of 11% of the data is deleted in this step: 10% for spikes, and 1% for telemetry dropouts. Next, certain periods of data have excess noise, correlated with noise in the data from a cryogenic temperature sensor. This suggests an intermittent electrical problem as the common origin. An additional 13% of the data are cut based on the noise level in this sensor. Finally, we delete any chopper cycle in which any points are cut, thus eliminating an additional 6% of the data, for a total of 30% of the data deleted. The fractions of data deleted given above are relative to the total 5.0 h period of CMBR observations.

We perform two demodulations of the detector signals. The single difference demodulation takes the difference between the signal with the secondary to the right from that with the secondary to the left, making an antisymmetric beam pattern. The double difference takes the signal with the secondary centered and subtracts the signal with the secondary to either side, making a symmetric beam-pattern. We use our scan over Jupiter to choose demodulations optimized for signal to noise ratio.

We estimate the instrument noise by measuring the variance in 100 s segments of the demodulated data after removing a slow drift. For the double difference demodulation, the achieved sensitivity in each channel is 180, 160, 110, and $160 \mu\text{Ks}^{1/2}$ Rayleigh-Jeans; for the single difference it is 20% to 50% larger. For channels 1 and 2 this corresponds to 360 and $910 \mu\text{Ks}^{1/2}$ CMBR. The offset in the demodulated data in the various channels and demodulations ranges from 1 to 5 mK; the offset drift over the whole flight is small compared to this.

We divide the data into $0^\circ.12$ bins in sky position along RA and Dec, and 10° bins in angular orientation of the chopper direction on the sky (roll). We dedrift and bin the data by fitting the data for each channel to a model consisting of a brightness in each bin, plus a slowly varying function of time (a cubic spline with knots spaced at 5 min intervals). This is done separately for each channel and demodulation. The reduced χ^2 of these fits are 0.99–1.17.

The data are calibrated by our observations of Jupiter, using the values of the brightness temperature of Jupiter reported in Goldin *et al.* 1996 (of the two models presented in that paper, we use the temperatures based on the “Rudy model,” Rudy *et al.* 1987). The error in the calibration is estimated to be 5%, dominated by the uncertainty in the Jupiter temperature.

3.2. Spectral Decomposition

We derive measurements of CMBR anisotropy and ISM dust emission by fitting the four channels to a two-component spectral model. The first component is cosmic microwave background radiation with $T = 2.728$ K (Fixsen *et al.* 1996a), with the free parameter being the anisotropy ΔT ; and the second component is emission from dust in the interstellar medium, with the free parameter being the optical depth. The dust is assumed to have a temperature of 20 K and an emissivity spectral index of 1.5; we find that varying the spectral index from 1.3 to 2.0 has essentially no effect on the CMBR results, but does affect the dust results as noted below. The χ^2/DOF of this fit is 505/548 for the single difference demodulation, and 533/548 for the double difference, both entirely consistent with a χ^2 distribution.

The resulting measurement of interstellar dust optical depth is plotted in Fig. 1. We have fit these measurements to the *IRAS* Sky Survey Atlas (ISSA) at 100 μm (Wheelock *et al.* 1994) convolved with our beam patterns. In this fit we assume a dust temperature of 20 K, and find the best-fit optical depth ratio between 100 μm and 444 μm . Fig. 1 also shows this ISSA model. The χ^2 of this fit is 449/273 for the single difference demodulation, and 356/273 for the double difference. There is clear correlation between this measurement and the ISSA, but the improbable values of χ^2 indicate that they are not in complete agreement. From the results of this fit we can assign an effective dust emissivity spectral index between 100 μm and 444 μm of 1.46 ± 0.28 ; the error bar includes the effect of varying the assumed index in the spectral decomposition from 1.3 to 2.0. This measurement of index is consistent with our previous measurements (Papers I and II), and with measurements by the *COBE* FIRAS and *DIRBE* instruments over the entire sky (Reach *et al.* 1995).

The CMBR component is plotted in Fig. 2. For reference, the antenna pattern is also shown. The anisotropy is clearly visible. This dataset is considered further in the next subsection.

The procedure for producing figures 1 and 2 needs to be briefly explained. The dataset that results from our analysis is difficult to represent in a plot for three reasons: there are a large number of data points (275), it has a significantly non-diagonal covariance matrix, and it is a function of declination and roll as well as of right ascension. To make the figures, we do the following. First, we project out the eigenmodes of the covariance matrix with the largest eigenvalues (~ 10), from both the data and the covariance. This results in a nearly diagonal covariance, from which we estimate the error bars. We then rebin the data, ignoring declination and roll, and using coarser right ascension bins. These steps are performed only for making a representative and comprehensible visual presentation of the data; all analyses are done with the full dataset and covariance matrix.

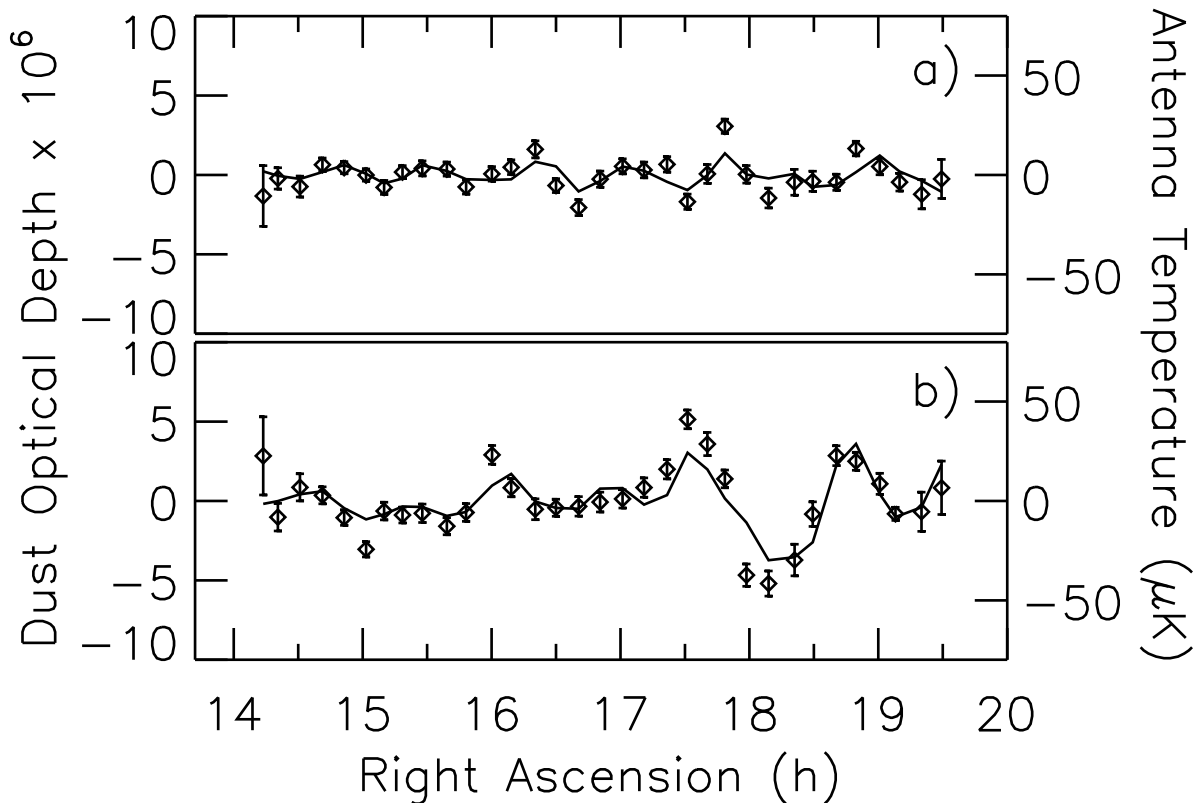


Fig. 1.— Optical depth of interstellar dust at 22.5 cm^{-1} . The right-hand scale is antenna temperature at 22.5 cm^{-1} . The points with error bars are our measurements. The curve is the ISSA 100 μm data convolved with our beam pattern, with amplitude fitted to our measurements. a) Double difference demodulation; b) single difference.

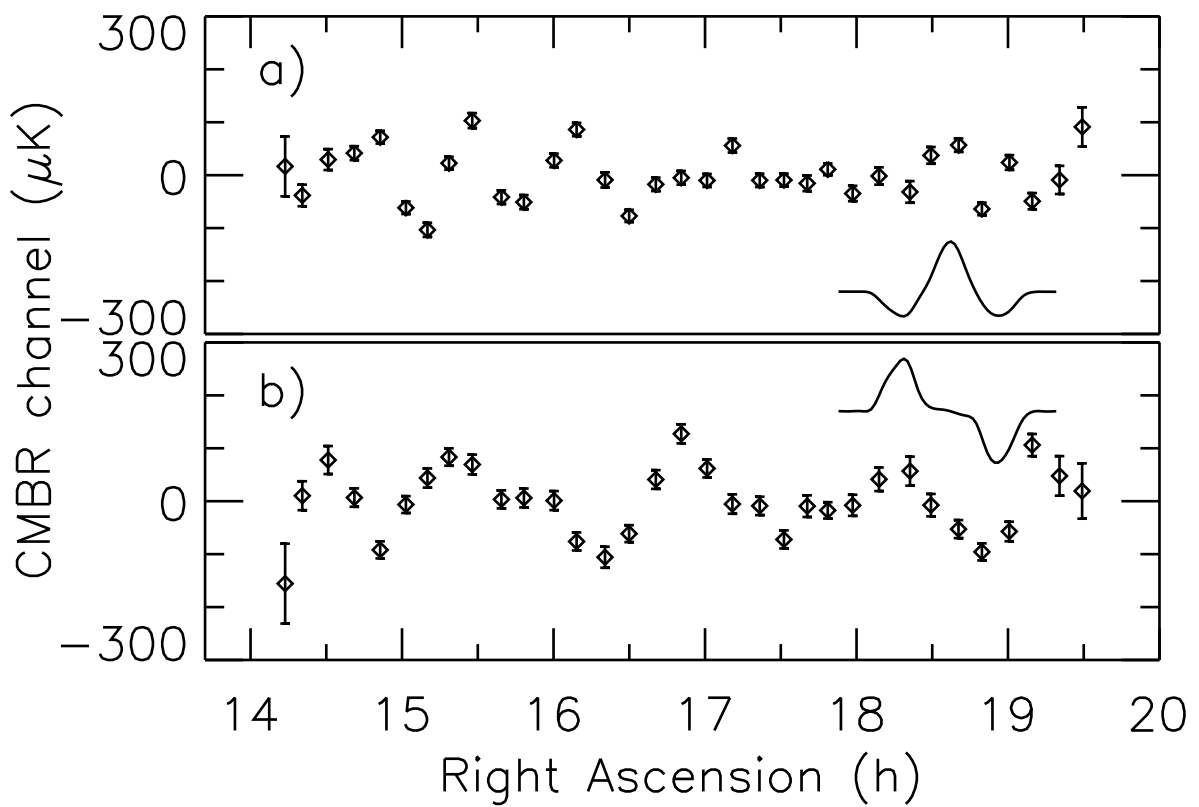


Fig. 2.— Our measurements of CMBR anisotropy. For reference, the beam pattern is superposed. a) Double difference demodulation; b) single difference.

3.3. CMBR Anisotropy

To assess the implications of these observations for cosmological parameters, we have used the same method as in Papers I and II. We choose a correlation function to test, and use the likelihood ratio statistic to find a 90% confidence interval on an overall multiplier of the correlation function. This confidence interval is bounded by the 95% confidence level upper and lower bounds. As in papers I and II, we have applied this test to Gaussian-shaped correlation functions of various correlation lengths. We have also tested a number of CDM models. In Papers I and II, we only presented results based on each demodulation separately; here we also present results based on both taken together.

The results from the Gaussian-shaped correlation functions, $C(\theta) \propto \exp[-(\theta/\theta_c)^2/2]$, are shown in Fig. 3. This figure shows limits for each demodulation, and for both demodulations taken together. The horizontal axis is the correlation length θ_c of the correlation function, and the vertical axis is total rms anisotropy, $[C(0)]^{1/2}$. Table 1 gives results for selected correlation lengths. Both the figure and the table show 90% confidence intervals.

We have also tested various adiabatic cold dark matter models using correlation functions computed with CMBFAST (Seljak and Zaldarriaga 1996). Starting from a nominal set of parameter values, we vary one parameter at a time, and find the interval of that parameter which produces correlation functions consistent with these measurements. The nominal set of parameters is $h = 0.5$, $\Omega = 1$, $\Omega_b h^2 = 0.0125$, $\Lambda = 0$, $Y_{\text{He}} = 0.24$, $n = 1$, and no early reionization, using only scalar perturbations. CMBFAST produces correlation functions which are normalized to DMR via the fitting function of Bunn and White 1997; this normalization has an uncertainty of 7%. We test correlation functions in the same way as above, with an overall multiplier as the free parameter. If the 90% confidence interval on this parameter, expanded by the combined calibration uncertainty of this experiment and the DMR normalization, does not include the value 1, then we reject that correlation function. To be conservative, we combine the normalization and calibration errors by adding, yielding 12%. In varying h , holding the other parameters fixed, we find that these data are consistent with $h < 0.78$. In varying the spectral index n of the initial perturbations, we find that it is constrained to $0.8 < n < 1.35$. To examine early reionization, we adopt a model that the ionization fraction goes suddenly from 0 to 1 at some redshift z ; we find that $z < 56$. This corresponds to an optical depth τ to the last scattering surface of $\tau < 0.37$.

We compute the band power estimator of Bond (Bond 1995) by hypothesizing a correlation function $C_l = 6C_2/l(l+1)$ and using the above procedure to place limits on

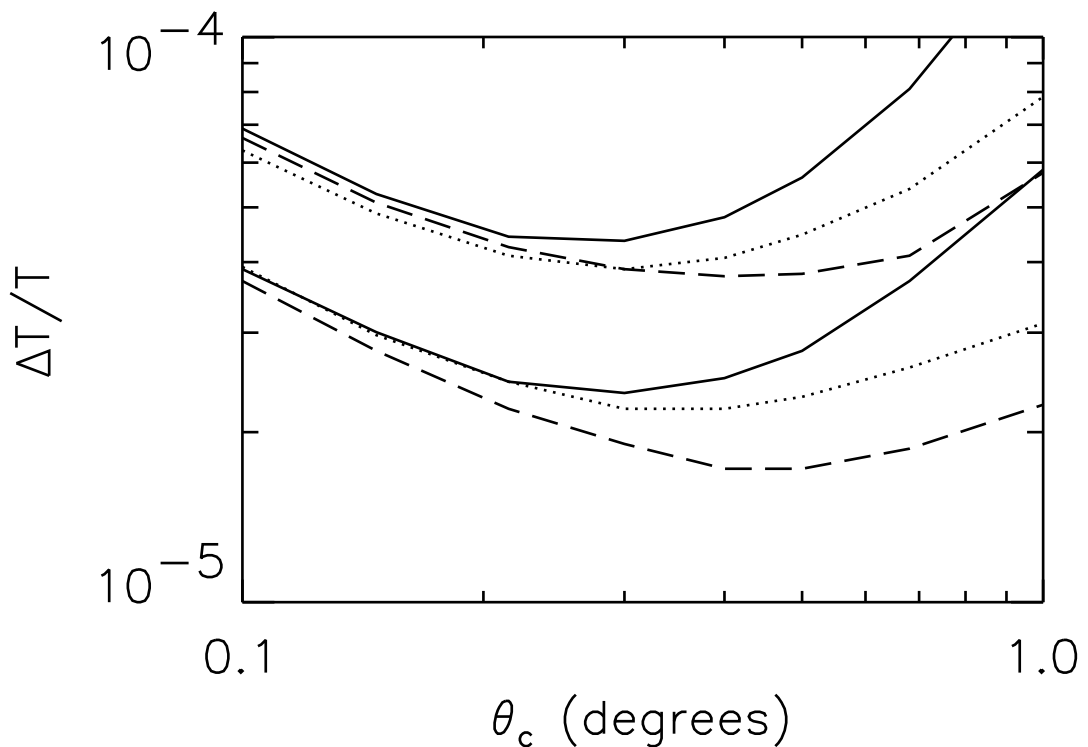


Fig. 3.— Limit on total rms anisotropy for Gaussian-shaped correlation functions. Each limit is a 95% confidence level; an upper and lower bound together limit a 90% confidence interval. Shown are upper and lower limits for the double difference demodulation (solid lines); upper and lower limits for the single difference demodulation (dashed); and upper and lower limits for both demodulations (dotted). The calibration error is not included in these limits.

C_2 ; then the band power estimator $\langle \delta T \rangle \equiv \langle l(l+1)C_l/2\pi \rangle^{1/2} = \sqrt{3/\pi}C_2^{1/2}$. To produce 1σ bounds, we compute 84% confidence level upper and lower bounds; the central value is the median (50% confidence level bound). For the single difference demodulation, we find that $\langle \delta T \rangle = 50_{-11}^{+16} \mu\text{K}$, at a mean $l = 160$; and for the double difference demodulation, $\langle \delta T \rangle = 65_{-13}^{+18} \mu\text{K}$, at a mean $l = 270$ (both 1σ limits, including calibration error). We include calibration error in our limits by adding it to the statistical error (not in quadrature). The 1σ limits with statistical errors only are 50_{-9}^{+13} and $65_{-10}^{+14} \mu\text{K}$ respectively.

4. Conclusions

The MSAM1-95 data show a highly significant detection of CMBR anisotropy, consistent in amplitude with the MSAM1-92/MSAM1-94 measurements (Papers I and II). With our calibration error taken into account, the limits in Table 1 for both demodulation and the full dataset are, for Gaussian-shaped correlations functions with $\theta_c = 0^\circ 3$, $2.2 \times 10^{-5} < \Delta T/T < 3.9 \times 10^{-5}$ (90% confidence interval).

In Paper II, we reserved judgment about the repeatability of our single difference measurement, but Inman *et al.* 1997 have shown that, for both demodulations, observations of the same field in 1992 and 1994 agree. This is a strong argument in favor of the reliability of MSAM1 data; therefore we now recommend without reservation the use of results based on both demodulations.

The band-power estimates for the single and double difference quoted above suggest a rise in the power spectrum from $l = 160$ to 270. However, the band-power estimate we quote for the double difference ($l = 270$) is 1.78σ larger than the MSAM1-94 measurement (Paper II); that measurement, converted to these units, is $\langle \delta T \rangle = 40_{-10}^{+12} \mu\text{K}$. The probability of a difference of this magnitude or greater is 7.5%, not small enough to call this an inconsistency. In this light we might ask if current measurements of band-power in this range of angular scale lend any weight to the hypothesis that the power spectrum is rising. Our present measurement of band-power at $l = 160$ is in agreement with the measurement of MSAM1-94, $\langle \delta T \rangle = 35_{-10}^{+14} \mu\text{K}$, and with the measurement by Python, $\langle \delta T \rangle = 58_{-13}^{+15} \mu\text{K}$ at $l = 180$ (Platt *et al.* 1997). Our measurement at $l = 270$ is in agreement with that by SK95, $\langle \delta T \rangle = 85_{-17}^{+23} \mu\text{K}$ at $l = 240$ (Netterfield *et al.* 1997, error bar adjusted to include calibration uncertainty); but as noted above, our MSAM1-94 measurement, while statistically consistent with these numbers, is rather smaller. These three experiments, taken together, suggest that there is a rise in the power spectrum from $l \sim 160$ to $l \sim 270$, but the statistical significance is modest. If we choose to ignore MSAM1-94, the suggestion is stronger, but the significance is still not compelling.

Our measurements of CMBR and dust will be made available on our FTP server, in
<ftp://cobi.gsfc.nasa.gov/pub/data/msam-jun95>.

This work would not be possible without the excellent support we receive from the staff of the National Scientific Balloon Facility. We thank G. Hinshaw and G. Wilson for illuminating discussions. Financial support was provided by the NASA Office of Space Science, under the theme “Structure and Evolution of the Universe.”

Table 1. Upper and lower bounds on total rms CMBR anisotropy ($\sqrt{C_0}$)

θ_c	Demodulation	Upper Bound (μK)	Lower Bound (μK)
0°5	Single	104	47
0°3	Double	118	63
0°5	Both	122	64
0°3	Both	107	61

Note. — The limits in this table do not include calibration uncertainty.

REFERENCES

Bond, J. R. 1995, *Astrophys. Lett. Commun.*, **32**, 63.

Bond, J. R. and Jaffe, A. H. 1997. Cosmic Parameter Estimation Combining Sub-Degree CMB Experiments with *COBE*. In *Microwave Background Anisotropies*, Proceedings of the 31st Moriond meeting. in press, preprint [astro-ph/9610091](#).

Bunn, E. F. and White, M. 1997, *ApJ*. in press, [astro-ph/9607060](#).

Cheng, E. S. *et al.* 1996, *ApJ*, **456**, L71.

Cheng, E. S. *et al.* 1994, *ApJ*, **422**, L37.

Fixsen, D. J., Cheng, E. S., Gales, J. M., Mather, J. C., Shafer, R. A., and Wright, E. L. 1996a, *ApJ*, **473**, 576.

Fixsen, D. J. *et al.* 1996b, *ApJ*, **470**, 63.

Goldin, A. B. *et al.* 1996, *ApJ*. submitted, preprint [astro-ph/9612040](#).

Inman, C. A. *et al.* 1997, *ApJ*, **478**, L1.

Netterfield, C. B., Devlin, M. J., Jarosik, N., Page, L., and Wollack, E. J. 1997, *ApJ*, **474**, 47.

Platt, S. R., Kovac, J., Dragovan, M., Peterson, J. B., and Ruhl, J. E. 1997, *ApJ*, **475**, L1.

Reach, W. T. *et al.* 1995, *ApJ*, **451**, 188.

Rudy, D. J., Muhleman, D. O., Berge, G. L., Jakosky, B. M., and Christensen, P. R. 1987, *Icarus*, **71**, 159.

Seljak, U. and Zaldarriaga, M. 1996, *ApJ*, **469**, 437.

Wheelock, S. L. *et al.* 1994. *IRAS Sky Survey Atlas Explanatory Supplement*. JPL Publication 94-11. JPL, Pasadena.